Side-Illuminated Photoconductive Semiconductor Switch Based on High Purity Semi-Insulating 4H-SiC

Pyeung Hwi Choi, Yong Pyo Kim, Min-Seong Kim, Jiheon Ryu, *Senior Member, IEEE*, Sung-Hyun Baek, Sung-Min Hong, *Member, IEEE*, Sungbae Lee, and Jae-Hyung Jang, *Senior Member, IEEE*

***Abstract*— High purity semi-insulating (HPSI) 4H-silicon carbide (SiC) was used to fabricate lateral and vertical photoconductive semiconductor switches (PCSSs). The lateral PCSSs were illuminated from the frontside (fPCSS) or the backside (bPCSS). The side-illuminated vertical PCSS (vPCSS) was designed to increase the light-matter interaction volume. A 532-nm pulsed laser with adjustable energy was utilized to excite the PCSSs. The turn-on time was found to be highly dependent on the optical illumination energy, and the full-width at half-maximum of the PCSSs output waveforms was related to the peak output voltage. The output electrical pulse from the vPCSS exhibited a shorter turn-on time and a larger pulsewidth than the two types of lateral PCSSs. The vPCSS outperformed the fPCSS and bPCSS in terms of minimum ON-state resistance and output pulse amplitude under the same optical illumination energy. The vPCSS, which utilizes a large effective contact area to collect photogenerated carriers, also had higher photon absorption efficiency by arranging the optical path at a right angle to the carrier transport. The vPCSS exhibited a minimum ON-state resistance of 0.34 Ω at optical illumination energy of 8 mJ.**

***Index Terms*— Frontside illumination backside illumination, high purity semi-insulating (HPSI) 4H-silicon carbide (SiC), photoconductive semiconductor switches (PCSSs), side illumination.**

Manuscript received August 14, 2021; revised September 25, 2021; accepted September 28, 2021. Date of publication October 13, 2021; date of current version December 1, 2021. This work was supported in part by the Agency for Defense Development and in part by the National Research Foundation of Korea (NRF) Grant funded by the Korea Government (Ministry of Science and ICT) under Grant 2017R1A2B3004049. The review of this article was arranged by Editor J. Huang. *(Corresponding author: Jae-Hyung Jang.)*

Pyeung Hwi Choi, Yong Pyo Kim, and Sung-Min Hong are with the School of Electrical Engineering and Computer Science, Gwangju Institute of Science and Technology (GIST), Gwangju 61005, Republic of Korea (e-mail: cph0618@gist.ac.kr).

Min-Seong Kim, Jiheon Ryu, and Sung-Hyun Baek are with the 1st R&D Institute, Agency for Defense Development, Daejeon 34186, Republic of Korea.

Sungbae Lee is with the Department of Physics and Photon Science, Gwangju Institute of Science and Technology (GIST), Gwangju 61005, Republic of Korea.

Jae-Hyung Jang is with the School of Energy Engineering, Korea Institute of Energy Technology (KENTECH), Naju 58330, Republic of Korea (e-mail: jjang@kentech.ac.kr).

Color versions of one or more figures in this article are available at https://doi.org/10.1109/TED.2021.3117535.

Digital Object Identifier 10.1109/TED.2021.3117535

I. Introduction

PHOTOCONDUCTIVE semiconductor switches (PCSSs) have been investigated as promising optoelectronic devices for pulsed power systems since the late 1970s [1]. Compared to other high-power switches, such as the spark gap, insulated gate bipolar transistor (IGBT), and thyristor, PCSSs have unique advantages including ultrafast switching, reliable operation, and negligible jitter time. The solid-state microwave generation techniques using the PCSSs have attracted interest in applications, such as ultrawideband (UWB) and high-power microwave (HPM) generators [2]–[5]. The PCSS can operate in linear and nonlinear modes. The conductivity of PCSSs operating in the linear mode is proportional to the incident optical power, while the avalanche process dominates in the nonlinear mode, which is also called the high gain mode [6], [7].

Several semiconductor materials have been considered as candidates for PCSSs, including silicon (Si) [8], gallium arsenide (GaAs) [9], silicon carbide (SiC) [10], gallium nitride (GaN) [11], [12], and diamond [13]. Even though earlier works on GaAs-based lateral PCSSs reported high-voltage and high-current switching performances [14]–[16], there have been research activities to improve the operating voltages of PCSSs using wide bandgap semiconductors. GaN has excellent properties, with high breakdown field and high electron saturation velocity, but techniques to grow high-quality single-crystal GaN substrates are still under development. Synthetic diamond doped with nitrogen appeared as a new material for PCSSs, but its material properties, such as the nature of deep traps and carrier lifetimes, are still under investigation. SiC-based PCSSs have also been investigated to achieve higher operating voltages. The excellent material properties of SiC, such as wide bandgap energy (3.23 eV), high breakdown field (2–4 MV/cm), high electron saturation velocity (2.0×10^7 cm/s), and high thermal conductivity ($4.9\ \mathrm{W{\cdot}cm^{-1}K^{-1}}$), have driven active studies of SiC-based PCSSs in search of higher voltage, higher current, and more stable operations [17]–[19].

High purity semi-insulating (HPSI) 4H-SiC grown without using a deep level dopant became a probable material candidate of PCSSs due to its long recombination

lifetime (6.5 ns [20]) and high electron mobility ($\mu_{n\perp c}$ of 950, and $\mu_{n||c}$ of 1141 cm^2/V·s [17], [21]). Vanadium (V)-doped 6H-SiC, the other commonly used semi-insulating SiC, has been reported to have a shorter recombination lifetime of 160 ps [22] and lower mobility ($\mu_{n\perp c}$ of 415, and $\mu_{n||c}$ of 40 cm^2/V·s [17], [21], [23]) than 4H-SiC. The photoconductive gain is proportional to the ratio of the carrier lifetime to the carrier transit time [24]. Considering that the carrier transit time is inversely proportional to the electron drift velocity, and 4H-SiC has 1 $\sim$ 1.5 times higher electron drift velocity than 6H-SiC in a high electric field from 10^3 to 10^6 V/cm [17], HPSI 4H-SiC can achieve higher photoconductivity than V-doped 6H-SiC. Two types of lateral PCSSs based on HPSI 4H-SiC are excited by a 354-nm pulsed laser [25]. Conventional PCSS with a gap size of 0.81 mm switched a maximum voltage of 10 kV into a 50-Ω load with a peak current of 182 A, and the radial-type backside-illuminated PCSS switched a maximum voltage of 30 kV into a 30-Ω load with a peak current of 938 A. Considering that the penetration depth of 354-nm light into 4H-SiC is 48 μm, optical absorption takes place near the illumination surface in these devices. Because the radial devices are illuminated from the backside with a 354-nm laser, the substrate thicknesses were limited to less than 100 μm [25]. Even though top- and backside-illuminated lateral devices and vertical devices are presented in [25], the detailed comparative studies are still lacking, and the pulsed output performance of the vertical devices was not presented. Another top-illuminated lateral PCSS based on HPSI 4H-SiC with a gap size of 1 mm was reported [26]. When a 355-nm laser having pulsed energy as high as 10.5 mJ was utilized for the optical excitation, the minimum ON-state resistance lower than 1 Ω was obtained at a bias voltage of 6 kV. A highly doped n-GaN layer was grown on top of SiC substrate to improve the ohmic contact performance of the electrodes, which helped to lower the minimum ON-state resistance [26].

The lateral PCSS, where two electrodes are placed side by side on the surface of the semiconducting substrate, is prone to surface flashover because the electric field is concentrated at the edge of the electrodes. To overcome this drawback of the lateral PCSS, SiC-based vertical PCSSs (vPCSSs), where the two electrodes are placed on opposite surfaces of the substrate, have also been reported [27]–[31]. The vPCSS has the advantages of distributing currents to a large electrode area and suppressing the electric field at the edge of the electrodes. However, earlier vPCSS based on SiC exhibited limitations in high-voltage switching, due to the micropipe defects in SiC substrates [25]. Recent advances in SiC substrates have resulted in dramatically reduced micropipe defect density, lower than 0.1 cm^{-2}, so that it is now possible to fabricate vPCSS on SiC for high-voltage switching.

There are two types of illumination strategies for vPCSSs. The laser light can be introduced to the vPCSS by surface normal illumination or side illumination. A transparent conductive window is introduced on one of the electrodes in the vPCSS for the surface normal illumination [28]–[30]. Because the devices were illuminated by the 532-nm laser light, they suffer from low optical absorption efficiency. To overcome this drawback, a highly reflective silver mirror was integrated on the backside electrode [29], [30], which doubles the optical path length leading to the optical absorption efficiency enhancement. The other configuration is the side-illuminated vPCSS, where the light is introduced via a side facet of the device. This can increase the photon absorption efficiency due to the longer optical path. By arranging the optical path at a right angle to the carrier transport direction, the tradeoff between the photon absorption efficiency and the carrier transit time can be overcome. Side-illuminated vPCSSs can also utilize the entire electrode area for photogenerated carrier collection. Sullivan [31] tested V-doped 6H-SiC-based vPCSSs with side illumination on the two opposite facets of the 1-mm-thick substrate, with optical excitation from a 532-nm laser [31]. The devices exhibited a minimum ON-state resistance, $R_{\mathrm{ON,min}}$, of 0.66 Ω, and high current switching (1.4 kA) at a high hold-off voltage (17 kV). These output characteristics of the side illuminated vPCSS based on HPSI 4H-SiC, which has higher electron mobility perpendicular to the c-axis and longer recombination lifetime than VCSI 6H-SiC, suggest it is worth further investigation.

In this work, lateral PCSSs and side-illuminated vPCSS based on HPSI 4H-SiC were fabricated to investigate the impact of the device structures on the performance of the PCSSs. To achieve a more uniform optical absorption in the whole volume of the side-illuminated vPCSS device, the 532-nm laser was utilized for the optical excitation. The turn-on time was found to be highly dependent on the illuminated optical energy, and the full-width at half-maximum (FWHM) of the electrical pulses is dependent on the peak output voltage ($V_{o,\mathrm{peak}}$). The side-illuminated vPCSS outperformed the lateral PCSSs in terms of $R_{\mathrm{ON,min}}$, photon absorption efficiency, and hold-off voltages.

II. Experimental Setup

The lateral and vPCSSs were fabricated on 500-μm-thick HPSI 4H-SiC substrates with a resistivity higher than 10^7 Ω·cm and a micropipe density of 0.1 cm^{-2}. Metal electrodes were patterned by optical lithography, and a Ni/Ti/Au (40/40/150 nm) metallization was evaporated and lifted off, followed by rapid thermal annealing. For the lateral PCSSs, anode and cathode electrodes (5×2 mm^2) with a 500-μm-gap were laterally formed on the same side of the substrate, as shown in Fig. 1(a) and (b). Both electrodes were connected to the microstrip transmission line on the printed circuit board (PCB) by ribbon bonding. As shown in Fig. 1(c) and (d), the 8-mm-diameter circular electrodes were formed on both sides of the 1.3×1.3 cm^2 substrate for the vPCSS. The device was sandwiched using indium-coated copper bolts and nuts, and was electrically connected to a flexible PCB (F-PCB) so that the device could be mounted at a right angle to the rigid PCB board.

Fig. 2(a) illustrates the optical trigger setup for the PCSS devices. The second-harmonic Nd:YAG laser (Brilliant EaZy, Quantel) generates a 532-nm optical pulse with a beam diameter of 5.18 mm, an FWHM of 2.9 ns, at a repetition rate of 10 Hz. Wave plate and polarizing beam splitter cubes are employed to vary the optical energy from 590 nJ

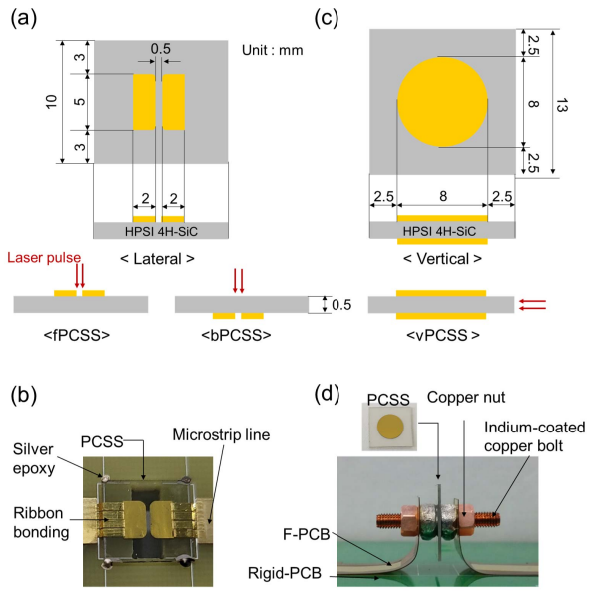

Fig. 1. Schematics of HPSI 4H-SiC PCSSs: (a) lateral PCSS with frontside illumination (fPCSS) and backside illumination (bPCSS) and (b) vPCSS. Pictures of the device modules: (c) lateral PCSS mounted on a rigid PCB and (d) vPCSS mounted with indium-coated copper bolts on an F-PCB.

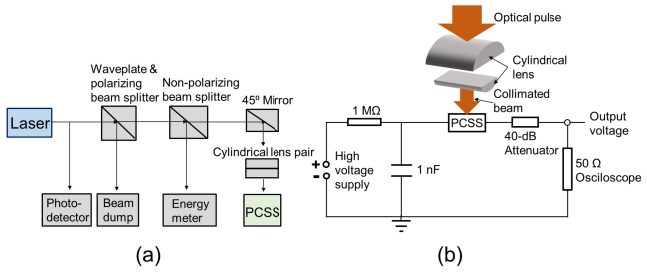

Fig. 2. (a) Optical trigger setup. (b) 4H-SiC PCSS test circuit with cylindrical lens pair for beam size conversion.

to 8 mJ. Another beam splitter is utilized to measure the optical energies, utilizing an energy meter (J-25 MB-HE, J-10 MB-LE, Coherent).

The circular laser beam was converted into a collimated elliptical beam by two cylindrical lenses with a focal length ratio of 10:1. The collimated laser beam was illuminated on the area between the electrodes of the lateral PCSS from the frontside (fPCSS) and backside of the devices (bPCSS). For the vPCSS, the laser beam was introduced sideways so that the optical path and the electronic carrier transport were at the right angle.

The optoelectronic test circuit is shown in Fig. 2(b). The high-voltage supply charges the capacitor (1 nF) through a resistor (1 MΩ) with a charging time constant of 1 ms. When the laser beam triggers the PCSS, the charge stored in the capacitor begins to discharge through the PCSS. The electrical pulse is attenuated by a 40-dB coaxial attenuator (WA42-40-34, Weinschel) and then measured by a 50-Ω terminated digital phosphor oscilloscope (DPO-7254, Tektronix) with a bandwidth of 2.5 GHz. The laser pulse was measured

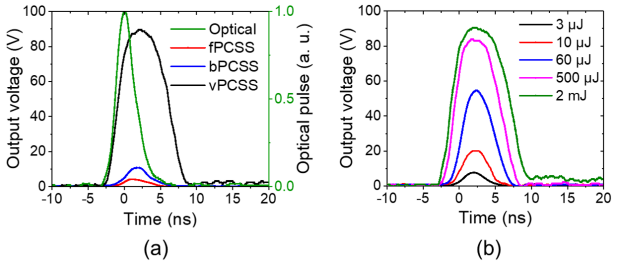

Fig. 3. (a) Optical pulse waveform from the 2-GHz Si photodetector and output voltage waveforms of the fPCSS, bPCSS, and vPCSS measured by 50-Ω terminated oscilloscope with optical energy of 1 mJ and a bias voltage of 100 V. (b) Output pulse waveforms of the vPCSS illuminated by various optical energies at a bias voltage of 100 V.

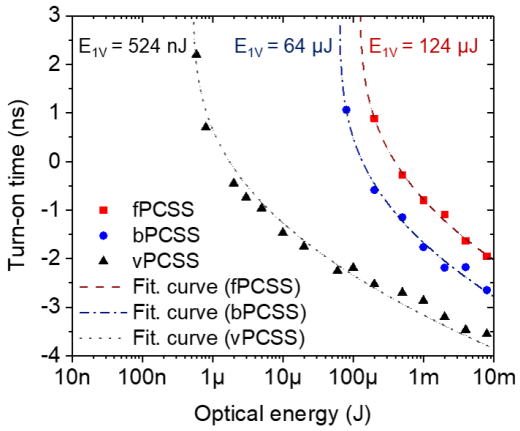

Fig. 4. Turn-on time (t_{ON}) depending on the triggering optical energy for the three types of PCSSs.

with a 2-GHz Si photodetector (DET025AL, Thorlabs) and was then utilized as a triggering signal for the output electrical pulse measurement. The noise floor of the output electrical pulse was measured to be 1 V.

III. Results and Discussion

The waveforms of the optical trigger pulse and output electrical pulses generated by the circuits, including the fPCSS, bPCSS, and vPCSS, are compared in Fig. 3(a). The dc voltage and illumination optical energies were 100 V and 1 mJ, respectively. The peak output voltage ($V_{o,\text{peak}}$) of the vPCSS circuit was 89.7 V, which was 9 and 22.5 times higher than those of bPCSS and fPCSS circuits, respectively. The FWHMs of the output pulses from the fPCSS, bPCSS, and vPCSS circuits were 4.08, 4.14, and 10.01 ns, respectively. The vPCSS showed an earlier turn-on response and larger output pulsewidth. The output energy of the single output pulse from the vPCSS was 142 and 935 times higher than those from the bPCSS and fPCSS, respectively.

Fig. 3(b) shows the output pulse waveforms of the vPCSS circuit under various optical illumination energies. It is interesting to observe that the turn-on time is dependent on the illumination optical energy. To quantitatively compare the turn-on characteristics shown in Fig. 4, the turn-on time, t_{ON}, was defined as the time instance when the output voltage reached 1 V. The laser pulses were utilized as the triggering

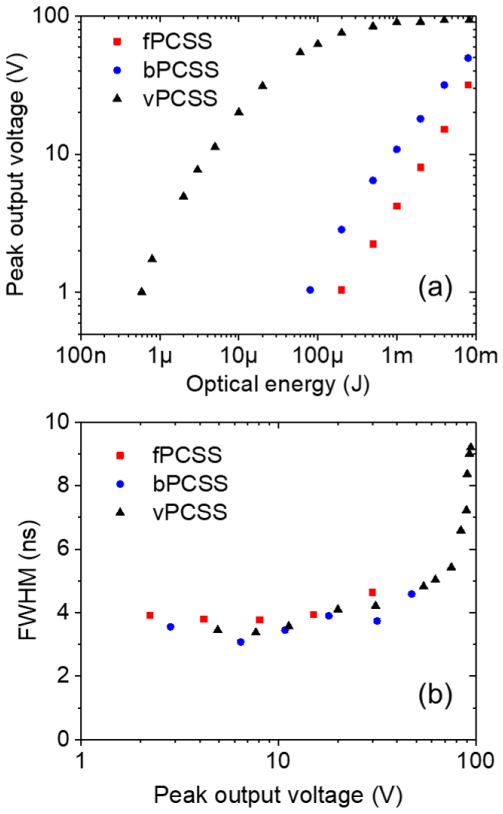

Fig. 5. (a) Peak output voltages of the fPCSS, bPCSS, and vPCSS with various optical energies at the bias voltage of 100 V. (b) FWHM of output pulses from the HPSI 4H-SiC PCSSs as a function of the peak output voltage at the bias voltage of 100 V.

signal for the oscilloscope. For the curve fitting, the optical pulse was assumed to have a Gaussian function, P_{opt}, as follows:

$$P_{\text{opt}}(t) = E_i \frac{1}{\sqrt{2\pi\sigma^2}} e^{\frac{-(t-t_0)^2}{2\sigma^2}} \tag{1}$$

where E_i is the optical energy of each optical pulse, t_0 is the time for the peak optical pulse power, which is 0, and σ is the optical pulsewidth of 1.146 ns. The turn-on energy, $E_{1\text{V}}$, which is the optical energy required to generate a $V_{o,\text{peak}}$ of 1 V, can be calculated as follows:

$$E_{1\text{V}} = \int_{-\infty}^{t_{\text{ON}}} P_{\text{opt}}(t)dt = \frac{1}{2}E_i\left(1 + \text{erf}\left(\frac{t_{\text{ON}} - t_0}{\sigma\sqrt{2}}\right)\right). \tag{2}$$

Then, from (2), t_{ON} can be expressed as

$$t_{\text{ON}} = \sigma\sqrt{2}\text{erf}^{-1}\left(\frac{2E_{1\text{V}}}{E_i} - 1\right) + t_0. \tag{3}$$

As shown in Fig. 4, the experimental results were fit by using (3). The fitting results show that $E_{1\text{V}}$'s of the fPCSS, bPCSS, and vPCSS are 124 μJ, 64 μJ, and 524 nJ, respectively. For all the PCSSs, as the optical energy increased, the turn-on time decreased. The vPCSS exhibited the lowest $E_{1\text{V}}$.

$V_{o,\text{peak}}$ of the output pulses with various optical energies is shown in Fig. 5(a). The vPCSS exhibited a higher $V_{o,\text{peak}}$ than the lateral PCSSs for all ranges of optical energy and showed

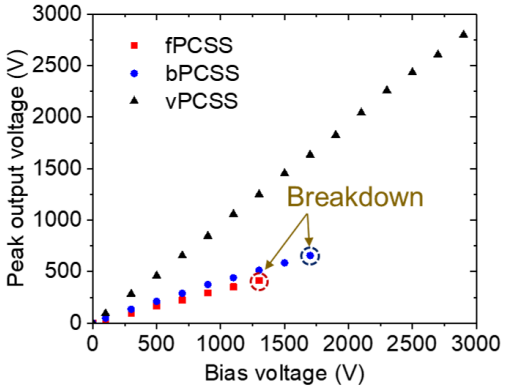

Fig. 6. Peak output voltages of the fPCSS, bPCSS, and vPCSS versus bias voltage at the optical energy of 8 mJ.

saturating behavior at optical energies higher than 500 μJ. This implies that the ON-state resistance of the vPCSS is far lower than the load resistance of 50 Ω. In Fig. 5(b), the FWHM of the output waveforms is shown as a function of $V_{o,\text{peak}}$. All three PCSSs showed similar pulse widths for the same $V_{o,\text{peak}}$. It shows that the FWHM is dependent on the peak output voltage rather than the PCSS structure or illumination strategies. When the circuits provide the same peak output voltage, the PCSS devices exhibit the same resistance value. It implies that the resistance value of the PCSS is the most important parameter, and the parasitic elements associated with the three types of devices do not play significant roles in determining the output pulse waveform for the experimental setup utilized in this study. The FWHM of the vPCSS exhibits dramatic increase, when the $V_{o,\text{peak}}$ gets higher than 84 V. The output voltage saturation by load resistance, as mentioned above, limits the increase of $V_{o,\text{peak}}$ and leads to the round shape around the peak, which can be observed in the output pulse waveforms in Fig. 3(b). The vPCSS exhibits a larger pulsewidth than the lateral PCSSs in Fig. 3(a) because vPCSS achieves a higher $V_{o,\text{peak}}$ than the lateral PCSSs at the same optical energy. The earlier turn-on response and higher output voltage of the vPCSS for the same laser pulse energy reveal that the vPCSS is a more sensitive and responsive switching device than the lateral PCSSs are.

Fig. 6 illustrates that $V_{o,\text{peak}}$ increases linearly with bias voltage. vPCSS exhibited a much higher $V_{o,\text{peak}}$ compared to the fPCSS and bPCSS at all bias voltages. The hold-off voltages of the fPCSS and bPCSS illuminated with optical energy of 8 mJ were 1.3 and 1.7 kV, respectively. At bias voltages higher than the hold-off voltage, both electrodes in the lateral PCSSs permanently broke down, as observed with the GaAs PCSSs [32]. Meanwhile, the vPCSS exhibited $V_{o,\text{peak}}$ of 2.8 kV at a bias voltage of 2.9 kV. The output pulse measurement at voltages higher than 3 kV was limited by the breakdown of the 50-Ω N-connector. This shows that the hold-off voltage of the vPCSS is higher than 3 kV.

The ON-state resistances of the PCSSs were calculated from the current by measuring the voltage across the 50-Ω load. The ON-state resistance, R_{ON}, of the PCSS is calculated

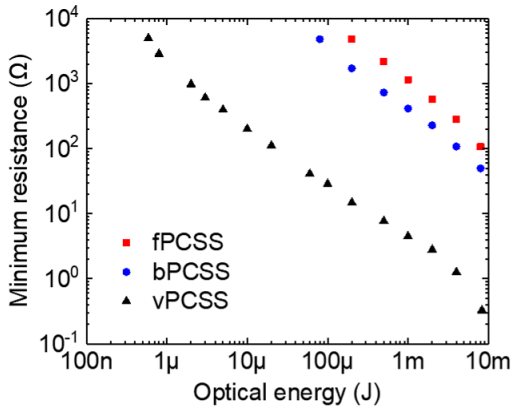

Fig. 7. Minimum ON-state resistances ($R_{ON,min}$) of the HPSI 4H-SiC PCSSs with various optical energies at bias voltages of 100 V.

with the following equation:

$$R_{ON} = \frac{V_{anode} - V_{cathode}}{I_{PCSS}} \tag{4}$$

where I_{PCSS} is the current along with the PCSS device, and V_{anode} and $V_{cathode}$ are voltages at the cathode and anode of the PCSS, respectively. V_{anode} is identical to the capacitor voltage discharged until time t and can be calculated as

$$V_{anode}(t) = V_{bias} - \int_0^t \frac{I_{PCSS}(t')}{C} dt' \tag{5}$$

where V_{bias} is the dc bias voltage applied by the high-voltage supply.

Fig. 7 shows the minimum ON-state resistances, $R_{ON,min}$, of the fPCSS, bPCSS, and vPCSS illuminated by various optical energies at a bias voltage of 100 V. The vPCSS exhibited the lowest $R_{ON,min}$ for all ranges of optical energy. When the optical energy of 8 mJ was applied to the device, the vPCSS achieved $R_{ON,min}$ of 0.34 Ω, the bPCSS exhibited 49.9 Ω, and the fPCSS did 108.8 Ω. $R_{ON,min}$ of the vPCSS was 1/153th of bPCSS's and 1/330th of the fPCSS's.

The reason for the lower $R_{ON,min}$ of the vPCSS compared to fPCSS and bPCSS may originate with a larger number of absorbed photons. Considering that the elliptical shape of the collimated laser beam has a width of 518 μm and the devices' illuminated area and optical path length, the relative number of absorbed photons of the three PCSSs can be calculated. The vPCSS absorbs 25.1 times more photons than the bPCSS and 26 times more than the fPCSS does. Therefore, the number of absorbed photons can only partially explain the superior performance of the vPCSS.

Another reason for the lower device resistance is the large effective contact area. In the case of bPCSS, since the laser beam size is larger than the electrode gap, the larger electrode area can be used as an effective contact area compared with the fPCSS. 3.5% of the laser beam energy can be illuminated on the back of the electrode area. $R_{ON,min}$ of the bPCSS was measured to be 1/2 of that of the fPCSS's. In addition, with the vPCSS, the optical pulse passed underneath the contact electrode by side illumination, utilizing the large electrode area as an effective contact area, so that the vPCSS exhibited significantly lower $R_{ON,min}$. The vPCSS also achieves higher photon absorption efficiency by arranging the optical path at a right angle to the electronic transport, as mentioned above, which leads to lower resistance in the vPCSS. The vPCSS, in this article, achieved $R_{ON,min}$ of 0.34 Ω at optical energy of 8 mJ.

TABLE I
$R_{ON,min}$ OF THE vPCSSs BASED ON SiC

Illumination method	Material type	$R_{on,min}$ (Ω)	Optical energy (mJ)	Ref.
Surface normal illumination w/ transparent window	VCSI 4H-SiC	7.5	65	[29]
Surface normal illumination w/ transparent window	VCSI 6H-SiC	5.6	31.9	[30]
Side-illumination	VCSI 6H-SiC	0.66	35.4	[31]
Side-illumination	HPSI 4H-SiC	0.34	8	This work

The performances of the SiC-based vPCSSs reported so far are compared in Table I. Cao *et al.* [29] reported a vPCSS based on V-compensated semi-insulating 4H-SiC, adopting a transparent window, and demonstrated $R_{ON,min}$ of 7.5 Ω at a bias voltage of 2 kV and optical energy of 65 mJ. It showed saturating behavior of $R_{ON,min}$ at optical energies higher than 25 mJ [29]. Wu *et al.* [30] reported a vPCSS based on VCSI 6H-SiC with a transparent window that exhibited $R_{ON,min}$ of 5.6 Ω at 2 kV with optical energy of 31.9 mJ [30]. Sullivan [31] reported a side-illuminated vPCSS based on V-compensated semi-insulating 6H-SiC. It achieved $R_{ON,min}$ of 0.66 Ω at a bias voltage of 270 V with optical energy of 35.4 mJ, which was calculated from peak optical power [31]. The HPSI 4H-SiC-based vPCSS, reported in this article, outperforms the other vPCSSs, reported in the literature, in terms of $R_{ON,min}$ even at the lower optical illumination energy.

IV. Conclusion

The output characteristics of PCSSs based on HPSI 4H-SiC, one with a lateral structure for frontside illumination and backside illumination, and the other with a vertical structure for side illumination, were investigated. The vPCSS exhibited much earlier turn-on behavior and a larger pulsewidth than the lateral PCSSs. The side-illuminated vPCSS has a large effective contact electrode area and increased photon absorption efficiency. By arranging the optical path at a right angle with the electronic transport, $R_{ON,min}$ of 0.34 Ω was achieved at optical energy of 8 mJ. This achieved $R_{ON,min}$ was lower than that of the previously reported vPCSS performance, even with lower optical illumination energy.

References

[1] P. LeFur and D. H. Auston, "A kilovolt picosecond optoelectronic switch and Pockel's cell," *Appl. Phys. Lett.*, vol. 28, no. 1, pp. 21–23, Jan. 1976, doi: 10.1063/1.88565.

[2] J. S. H. Schoenberg, J. W. Burger, J. S. Tyo, M. D. Abdalla, M. C. Skipper, and W. R. Buchwald, "Ultra-wideband source using gallium arsenide photoconductive semiconductor switches," *IEEE Trans. Plasma Sci.*, vol. 25, no. 2, pp. 327–334, Apr. 1997, doi: 10.1109/27.602507.

[3] L. Hu, J. Su, R. Qiu, and X. Fang, "Ultra-wideband microwave generation using a low-energy-triggered bulk gallium arsenide avalanche semiconductor switch with ultrafast switching," *IEEE Trans. Electron Devices*, vol. 65, no. 4, pp. 1308–1313, Apr. 2018, doi: 10.1109/TED.2018.2802642.

[4] Q. Wu, Y. Zhao, T. Xun, H. Yang, and W. Huang, "Initial test of optoelectronic high power microwave generation from 6H-SiC photoconductive switch," *IEEE Electron Device Lett.*, vol. 40, no. 7, pp. 1167–1170, Jul. 2019, doi: 10.1109/LED.2019.2918954.

[5] C. Luan, J. Zhao, L. Xiao, Q. Yang, X. Ma, and H. Li, "All solid-state electromagnetic pulse simulator based on the 4H-SiC photoconductive semiconductor switch," *Rev. Sci. Instrum.*, vol. 91, no. 1, Jan. 2020, Art. no. 014701, doi: 10.1063/1.5128450.

[6] W. Shi, X. Wang, and L. Hou, "Lower bound of electrical field for maintaining a GaAs photoconductive semiconductor switch in high-gain operating mode," *IEEE Trans. Electron Devices*, vol. 60, no. 4, pp. 1361–1364, Apr. 2013, doi: 10.1109/TED.2013.2244094.

[7] Z. Hemmat, R. Faez, E. Moreno, F. Rasouli, F. Radfar, and M. Zaimbashi, "Transient and steady state study of a rear-illuminated 6H-SiC photoconductive semiconductor switch," *Optik*, vol. 127, no. 11, pp. 4615–4620, Jun. 2016, doi: 10.1016/j.ijleo.2016.01.174.

[8] G. M. Loubriel *et al.*, "Long-lifetime silicon photoconductive semiconductor switches," *Proc. SPIE*, vol. 1873, pp. 27–38, Jun. 1993, doi: 10.1117/12.146560.

[9] G. M. Loubriel *et al.*, "Longevity of optically activated, high gain GaAs photoconductive semiconductor switches," *IEEE Trans. Plasma Sci.*, vol. 26, no. 5, pp. 1393–1402, Oct. 1998, doi: 10.1109/27.736024.

[10] S. Doğan, A. Teke, D. Huang, and H. Morkoç, "4H--SiC photoconductive switching devices for use in high-power applications," *Appl. Phys. Lett.*, vol. 82, no. 18, pp. 3107–3109, May 2003, doi: 10.1063/1.1571667.

[11] O. Imafuji, B. P. Singh, Y. Hirose, Y. Fukushima, and S. Takigawa, "High power subterahertz electromagnetic wave radiation from GaN photoconductive switch," *Appl. Phys. Lett.*, vol. 91, no. 7, Aug. 2007, Art. no. 071112, doi: 10.1063/1.2771528.

[12] J. H. Leach, R. Metzger, E. A. Preble, and K. R. Evans, "High voltage bulk GaN-based photoconductive switches for pulsed power applications," *Proc. SPIE*, vol. 8625, Mar. 2013, Art. no. 86251Z, doi: 10.1117/12.2005548.

[13] D. L. Hall *et al.*, "Photoconductive switch with high sub-bandgap responsivity in nitrogen-doped diamond," *IEEE Electron Device Lett.*, vol. 41, no. 7, pp. 1070–1073, Jul. 2020, doi: 10.1109/LED.2020.2999821.

[14] M. D. Pocha and R. L. Druce, "35-kV GaAs subnanosecond photoconductive switches," *IEEE Trans. Electron Devices*, vol. 37, no. 12, pp. 2486–2492, Dec. 1990.

[15] W. Shi, L. Tian, Z. Liu, L. Zhang, and Z. Zhang, "30 kV and 3 kA semi-insulating GaAs photoconductive semiconductor switch," *Appl. Phys. Lett.*, vol. 92, no. 4, pp. 92–95, Feb. 2008, doi: 10.1063/1.2838743.

[16] W. Shi and Z. Fu, "2-kV and 1.5-kA semi-insulating GaAs photoconductive semiconductor switch," *IEEE Electron Device Lett.*, vol. 34, no. 1, pp. 93–95, Jan. 2013, doi: 10.1109/LED.2012.2226558.

[17] M. Roschke and F. Schwierz, "Electron mobility models for 4H, 6H, and 3C SiC," *IEEE Trans. Electron Devices*, vol. 48, no. 7, pp. 1442–1447, Jul. 2001, doi: 10.1109/16.930664.

[18] M. E. Levinshtein, S. L. Rumyantsev, and M. S. Shur, *Properties of Advanced Semiconductor Materials*. New York, NY, USA: Wiley, 2001.

[19] C.-M. Zetterling, Ed., *Process Technology for Silicon Carbide Devices*. London, U.K.: INSPEC, 2002.

[20] C. Hettler, C. James, J. Dickens, and A. Neuber, "Carrier lifetime studies of semi-insulating silicon carbide for photoconductive switch applications," in *Proc. IEEE Int. Power Modulator High Voltage Conf. (IPMHVC)*, May 2010, pp. 34–37, doi: 10.1109/IPMHVC.2010.5958289.

[21] M. Bakowski, U. Gustafsson, and U. Lindefelt, "Simulation of SiC high power devices," *Phys. Status Solidi*, vol. 162, no. 1, pp. 421–440, Jul. 1997, doi: 10.1002/1521-396X(199707)162:1<421::AID-PSSA421>3.0.CO;2-B.

[22] G. Tamulaitis, I. Yilmaz, M. S. Shur, T. Anderson, and R. Gaska, "Carrier lifetime in conductive and vanadium-doped 6H-SiC substrates," *Appl. Phys. Lett.*, vol. 84, no. 3, pp. 335–337, Jan. 2004, doi: 10.1063/1.1641172.

[23] M. Ruff, H. Mitlehner, and R. Helbig, "SiC devices: Physics and numerical simulation," *IEEE Trans. Electron Devices*, vol. 41, no. 6, pp. 1040–1054, Jun. 1994, doi: 10.1109/16.293319.

[24] S. L. Chuang, *Physics of Photonic Devices*, 2nd ed. Hoboken, NJ, USA: Wiley, 2009, pp. 49–50.

[25] D. Mauch, C. White, D. Thomas, A. Neuber, and J. Dickens, "Overview of high voltage 4H-SiC photoconductive semiconductor switch efforts at Texas tech university," in *Proc. IEEE Int. Power Modulator High Voltage Conf. (IPMHVC)*, Jun. 2014, pp. 23–26, doi: 10.1109/IPMHVC.2014.7287198.

[26] L. Xiao *et al.*, "Effect of electron avalanche breakdown on a high-purity semi-insulating 4H-SiC photoconductive semiconductor switch under intrinsic absorption," *Appl. Opt.*, vol. 57, no. 11, pp. 2804–2808, Apr. 2018, doi: 10.1364/ao.57.002804.

[27] J. S. Sullivan and J. R. Stanley, "Wide bandgap extrinsic photoconductive switches," *IEEE Trans. Plasma Sci.*, vol. 36, no. 5, pp. 2528–2532, Oct. 2008, doi: 10.1109/TPS.2008.2002147.

[28] L. Wang *et al.*, "Effects of high-field velocity saturation on the performance of V-doped 6H silicon-carbide photoconductive switches," *IEEE J. Emerg. Sel. Topics Power Electron.*, vol. 9, no. 4, pp. 4879–4886, Aug. 2021, doi: 10.1109/JESTPE.2020.3038561.

[29] P. Cao, W. Huang, H. Guo, and Y. Zhang, "Performance of a vertical 4H-SiC photoconductive switch with AZO transparent conductive window and silver mirror reflector," *IEEE Trans. Electron Devices*, vol. 65, no. 5, pp. 2047–2051, May 2018, doi: 10.1109/TED.2018.2815634.

[30] Q. Wu, T. Xun, Y. Zhao, H. Yang, and W. Huang, "The test of a high-power, semi-insulating, linear-mode, vertical 6H-SiC PCSS," *IEEE Trans. Electron Devices*, vol. 66, no. 4, pp. 1837–1842, Apr. 2019, doi: 10.1109/TED.2019.2901065.

[31] J. S. Sullivan, "High power operation of a nitrogen doped, vanadium compensated, 6H-SiC extrinsic photoconductive switch," *Appl. Phys. Lett.*, vol. 104, no. 17, pp. 2–6, May 2014, doi: 10.1063/1.4875258.

[32] C. Ma, W. Shi, M. Li, H. Gui, N. Hao, and P. Xue, "Impact of current filaments on the material and output characteristics of GaAs photoconductive switches," *IEEE Trans. Electron Devices*, vol. 61, no. 7, pp. 2432–2436, Jul. 2014, doi: 10.1109/TED.2014.2323052.